VIP Conducting Perovskites Very Important Paper

International Edition: DOI: 10.1002/anie.201912575
German Edition: DOI: 10.1002/ange.201912575

High Compression-Induced Conductivity in a Layered Cu–Br Perovskite

*Adam Jaffe, Stephanie A. Mack, Yu Lin, Wendy L. Mao, Jeffrey B. Neaton, and Hemamala I. Karunadasa**

Abstract: *We show that the onset pressure for appreciable conductivity in layered copper-halide perovskites can decrease by ca. 50 GPa upon replacement of Cl with Br. Layered Cu–Cl perovskites require pressures > 50 GPa to show a conductivity of 10^{-4} S cm^{-1}, whereas here a Cu–Br congener, $(EA)_2CuBr_4$ (EA = ethylammonium), exhibits conductivity as high as 2×10^{-3} S cm^{-1} at only 2.6 GPa, and 0.17 S cm^{-1} at 59 GPa. Substitution of higher-energy Br 4p for Cl 3p orbitals lowers the charge-transfer band gap of the perovskite by 0.9 eV. This 1.7 eV band gap decreases to 0.3 eV at 65 GPa. High-pressure X-ray diffraction, optical absorption, and transport measurements, and density functional theory calculations allow us to track compression-induced structural and electronic changes. The notable enhancement of the Br perovskite's electronic response to pressure may be attributed to more diffuse Br valence orbitals relative to Cl orbitals. This work brings the compression-induced conductivity of Cu-halide perovskites to more technologically accessible pressures.*

Introduction

Layered or two-dimensional (2D) Cu–Cl perovskites are translucent yellow insulators. These crystalline solids have been examined under pressure for decades, revealing their pronounced structural and electronic evolution upon compression.[1] Motivation for their study has come, in part, from their similarities to the cuprate superconductors, whose critical temperatures (T_c) show a large pressure response.[2] In addition, the possibility of mechanically suppressing the Jahn–Teller (JT) distortion of the Cu^{II} ions has spurred numerous high-pressure studies.[1] This JT distortion results from the Cu $3d^9$ electronic configuration that drives a tetragonal elongation of the corner-sharing Cu–X (X = halide) octahedra (Figure 1 A,B), where the elongated bonds lie along the inorganic sheets. The singly occupied Cu $d_{x^2-y^2}$ orbitals could produce a half-filled band conducive for electronic transport. However, Cu–X perovskites remain insulating because this conduction pathway is disrupted by the antiferrodistortive alignment of the elongated X–Cu–X axes (Figure 1 B), resulting in orthogonal Cu $d_{x^2-y^2}$ orbitals.[3] The poor overlap between copper-derived half-filled orbitals therefore yields an electronic structure that is almost molecular in nature. Indeed, 2D Cu–X perovskites order ferromagnetically within their inorganic layers below T_c values as high as 72 K due to the orthogonality of the Cu $d_{x^2-y^2}$ orbitals containing unpaired spins.[4] Importantly, the entire 2D Cu-X perovskite family contains structurally analogous inorganic layers and similar electronic structures. Prior efforts to remove this orbital orthogonality through compression of Cu–Cl perovskites such as $(EA)_2CuCl_4$ and its congeners[1a,c] have elicited strong structural and piezochromic responses, indicating changes in orbital interactions that modulate electronic structure. At ca. 4 GPa, 2D Cu–Cl perovskites turn from translucent yellow to red likely due to the reduction of the ligand-to-metal charge-transfer (LMCT) band gap. Structural studies at these pressures have provided evidence for phase transitions resulting in octahedral tilting (rotations),[1b,d,e] which can induce partial overlap between Cu $d_{x^2-y^2}$-derived orbitals. However, the materials remained insulating at these pressures. We reported the first example of electronic transport in a layered Cu–Cl perovskite, albeit at very high pressure.[1f] This conductivity was attributed to a combination of Cu–Cl bond compression and octahedral tilting, which in concert could provide a conduction pathway through partial overlap of half-filled orbitals. By ca. 12 GPa, the Cu–Cl perovskite $(EDBE)CuCl_4$ (EDBE = 2,2′-(ethylenedioxy)bis(ethylammonium)) appeared opaque black and at 51 GPa a maximum conductivity of 2.9×10^{-4} S cm^{-1} was measured with an activation energy of conduction (E_a) of 0.218(5) eV.[1f] Herein, we show that the pressure required to obtain appreciable electronic conductivity in Cu–X layered perovskites can be reduced by ca. 50 GPa upon replacement of Cl with Br, attributed to the more diffuse Br valence

[*] Dr. A. Jaffe, Prof. H. I. Karunadasa
Department of Chemistry, Stanford University
Stanford, CA 94305 (USA)
E-mail: hemamala@stanford.edu
S. A. Mack, Prof. J. B. Neaton
Department of Physics, University of California Berkeley
Berkeley, CA 94720 (USA)
and
Materials Sciences Division, Lawrence Berkeley National Laboratory
Berkeley, CA 94720 (USA)
Dr. Y. Lin, Prof. W. L. Mao, Prof. H. I. Karunadasa
Stanford Institute for Materials and Energy Sciences, SLAC National Accelerator Laboratory
Menlo Park, CA 94025 (USA)
Prof. W. L. Mao
Department of Geological Sciences, Stanford University
Stanford, CA 94305 (USA)
Prof. J. B. Neaton
Kavli Energy NanoScience Institute, University of California Berkeley
Berkeley, CA 94720 (USA)
Supporting information and the ORCID identification number(s) for the author(s) of this article can be found under https://doi.org/10.1002/anie.201912575.

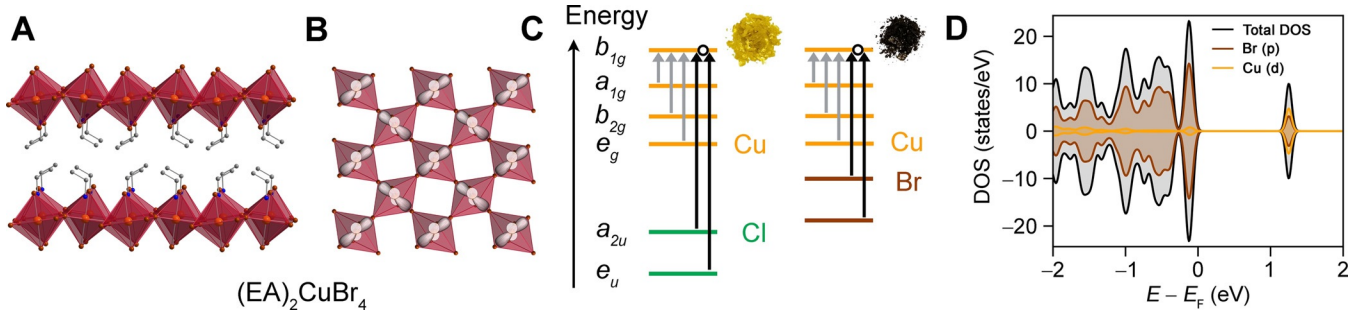

Figure 1. A) Single-crystal X-ray structure of $(EA)_2CuBr_4$ (EA = ethylammonium). Orange, brown, gray, and blue spheres represent Cu, Br, C, and N, respectively. H atoms omitted for clarity. B) A Cu–Br layer in $(EA)_2CuBr_4$ with schematic $d_{x^2-y^2}$ orbitals overlaid to illustrate their orthogonality. C) A schematic orbital energy diagram illustrating the electronic structures of 2D Cu–Cl (left) and Cu–Br (right) perovskites. The ligand-to-metal charge-transfer (LMCT) energies (black arrows) are substantially reduced upon replacement of Cl with Br, whereas the metal d–d transitions (gray arrows) remain relatively unchanged. Insets show photographs of $(EA)_2CuCl_4$ (yellow) and $(EA)_2CuBr_4$ (dark purple). D) Spin-polarized density of states (DOS) of $(EA)_2CuBr_4$ calculated with PBE using Tkatchenko-Scheffler van der Waals' corrections and $U = 8$ eV on the Cu d orbitals with in-plane antiferromagnetic ordering. The highest-energy filled state is set to zero. The computed DOS are consistent with the lower-energy Laporte forbidden predominantly Cu d–d transitions and the higher-energy dipole-allowed LMCT transitions observed in room-temperature optical spectra (Figure 3A).

orbitals capable of enhanced orbital overlap relative to Cl orbitals. Electronic conductivity as high as $1.98(8) \times 10^{-3}$ S cm^{-1} can be attained at only 2.6 GPa in a 2D Cu–Br perovskite, $(EA)_2CuBr_4$. The crystal structure of this 2D Cu–Br perovskite has not been reported previously, although its magnetic properties have been studied.[5] We contrast the compression-induced electronic properties of $(EA)_2CuBr_4$ with those of the previously reported Cu–Cl perovskites such as $(EA)_2CuCl_4$ and (EDBE)$CuCl_4$. Replacement of Cl with Br also yields a large decrease in the LMCT band gap from ca. 2.6 to 1.7 eV at ambient pressure. Compression of the Cu–Br perovskite affords a large band gap reduction, leading to a band gap of ca. 0.3 eV at 65 GPa, which is projected to close at 77 GPa.

Results and Discussion

Motivated to achieve the compression-induced electronic properties of Cu–Cl perovskites at more accessible pressures, we investigated the effects of replacing chlorides with heavier halides containing more diffuse orbitals to improve band dispersion through increased compression-induced orbital overlap. Copper-iodide perovskites are not known, likely due to the propensity of Cu^{2+} to oxidize I^-. We therefore explored the high-pressure properties of Cu–Br perovskites. Indeed, magnetic studies have shown significantly larger superexchange interactions in Cu–Br perovskites relative to the chlorides, attributed to the bromides' extended orbitals.[3a,6] The 2D Cu–Br perovskites are structurally analogous to the chlorides, yet only 11 are reported in the Cambridge Structural Database. To our knowledge, no investigations of their high-pressure properties have been reported.

For this study, we synthesized the 2D perovskite $(EA)_2CuBr_4$ (Figure 1A). The chloride analog, $(EA)_2CuCl_4$, exhibits an ambient-pressure bulk modulus (K_0) of 8.4 GPa,[1c] which is ca. 10–20 GPa lower than other Cu–Cl perovskites with organic monolayers (containing diammonium molecules) or inorganic cation layers.[1c,e,f,h] Lower K_0 values indicate greater compressibility, decreasing the pressure necessary to induce significant structural and electronic modification. Evaporation of a methanolic solution of (EA)Br and $CuBr_2$ (see Supporting Information for additional details) yields purple-gold plate-like crystals of $(EA)_2CuBr_4$ with metallic luster, whereas powder samples appear dark purple. The crystal structure of this 2D Cu–Br perovskite is structurally analogous to other Cu–X perovskites. A pronounced JT distortion of the metal-halide octahedra gives short and long Cu–Br distances of 2.4299(6) and 3.1404(6) Å, respectively.

Structural Response to Compression

We tracked the structural relaxation of $(EA)_2CuBr_4$ during compression in diamond-anvil cells (DACs) by measuring powder X-ray diffraction (PXRD) up to 64 GPa (Figures S1 and S2). With increasing pressure, the cell volume of the low-pressure α phase (space group: $P2_1/c$) is continuously reduced up to ca. 1.5 GPa. Above this pressure, a first-order crystalline phase transition is evident, which is complete after subsequent compression to 2.6 GPa (Figure S1). A similar first-order transition to a high-pressure phase occurs in 2D Cu–Cl perovskites at slightly higher pressures, ca. 3–4 GPa.[1] Based on observed reflections and systematic absences, we have indexed this high-pressure β phase in $(EA)_2CuBr_4$ to the orthorhombic *Cccm* space group although other space-group/unit-cell assignments are also possible. We also observe an increase in lattice stiffness above ca. 4 GPa, similar to the increased stiffness we reported for a Cu–Cl perovskite above ca. 8 GPa.[1f] This reduced compressibility is consistent with a second-order, isostructural phase transition to a high-pressure γ phase that retains the same lattice symmetry. This change in compressibility is illustrated by a fit of the measured pressure–volume relationship for $(EA)_2CuBr_4$ to the second-order Birch–Murnaghan equation of state (Figure 2). Within the β phase, we determine an ambient-pressure bulk modulus (K_0) of 12(2) GPa (Fig-

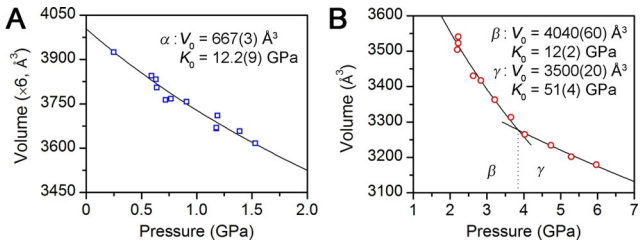

Figure 2. Unit-cell volume changes with pressure measured with X-ray diffraction for $(EA)_2CuBr_4$ for A) the low-pressure α phase ($P2_1/c$) and B) the high-pressure β and γ phases ($Cccm$). Second-order Birch–Murnaghan equation-of-state fits (black lines) and fit parameters are shown. Unit-cell volumes in (A) are multiplied by 6 for comparison with the β and γ phases.

ure 2B)—identical to the value of 12.2(9) GPa we find for the α phase (Figure 2A). However, above 4 GPa, we obtain $K_0 =$ 51(4) GPa for the γ phase from our measurements (Figure 2B), and we calculate a 2.5-fold decrease in compressibility. Our previous work on the Cu–Cl perovskite (EDBE)$CuCl_4$ elucidated a high-pressure γ phase with a K_0 of 59.2(9) above its apparent second-order transition at ca. 8 GPa.[1f] The similarity of this K_0 value to the measured K_0 for an individual $CuCl_6^{4-}$ octahedron of 63 GPa[1e] suggested that pressure-induced volume reduction in the γ phase of the perovskite was primarily associated with Cu–Cl bond compression. The K_0 of 51(4) for the γ phase of the Cu–Br perovskite similarly suggests that above ca. 4 GPa, within the γ phase, a large component of the volume reduction occurs through compression of the Cu–Br octahedra. Notably, octahedral compression appears to be more facile (lower K_0) and occurs at lower pressures (by ca. 4 GPa) in $(EA)_2CuBr_4$ compared to (EDBE)$CuCl_4$.

Above 6 GPa, another first-order crystalline phase transition to a high-pressure δ phase occurs that is marked by significant diffraction peak splitting, including the low-angle peaks just below 3° and 6° ($\lambda = 0.4979$ Å, Figure S2). Due to the relatively small number of discernible diffraction peaks and their broadness from 6 GPa up to 64 GPa, we were unable to reliably determine a space group for this δ phase. Peak broadness similarly precludes assessing if further phase transitions occur at higher pressure. However, a high degree of crystallinity is maintained up to the maximum measured pressure, evident from the retention of Bragg reflections, although the increase in broad baseline with compression may signal a small, partially amorphous component. Similar to other halide perovskites,[1f,7] releasing pressure leads to the recovery of the ambient-pressure α phase with minimal hysteresis (Figure S5).

Optical and Electronic Response to Compression

The weak, broad band centered at approximately 1.6 eV in the absorption spectra of $(EA)_2CuBr_4$ (Figure 3A) results from Laporte forbidden Cu d–d transitions between a_{1g}, b_{2g}, and e_g orbitals to the singly occupied b_{1g} orbital (Figures 1C and S6).[8] These transitions appear at similar energies to those of the analogous Cu–Cl perovskites, corroborating a predominantly metal-based origin. The stronger absorption onset at ca. 1.7 eV is assigned to $a_{2u} \rightarrow b_{1g}$ and $e_u \rightarrow b_{1g}$ ligand-to-metal charge-transfer (LMCT) transitions from orbitals with bromide p character (a_{2u} and e_u) to one with mostly Cu $d_{x^2-y^2}$ character (b_{1g}) (Figures 1C and S6).[1b,f,8] This LMCT band has a higher-energy onset of ca. 2.6 eV in Cu–Cl perovskites, due to the lower-energy Cl 3p orbitals compared to the Br 4p orbitals (Figure 1C). Thus, replacement of Cl with Br decreases the LMCT band gap by 0.9 eV, reflected in the color of these solids, with Cu–Cl perovskites appearing translucent yellow and Cu–Br perovskites appearing dark purple with a metallic luster (Figure 1C insets). With increasing pressure, we observe a large reduction of the band gap in $(EA)_2CuBr_4$ from 1.7 eV at ambient pressure to ca. 0.3 eV at 65 GPa (Figures 3 and S7). The rate of band gap change with pressure also tracks with the perovskite's structural relaxation, with changes in slope occurring at similar pressures to the α → β and γ → δ phase transitions. A simple linear extrapolation of the band gap as a function of pressure projects band gap closure at ca. 77 GPa.

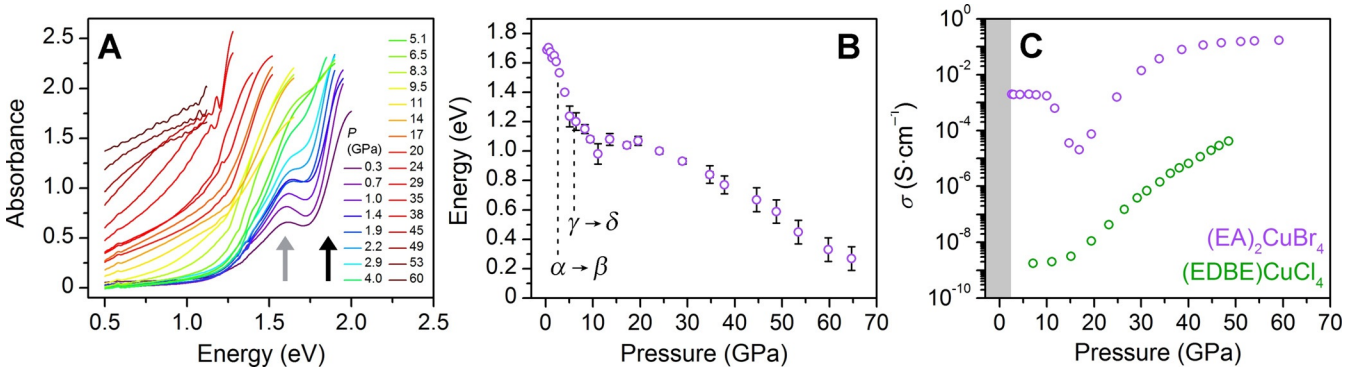

Figure 3. A) Variable-pressure absorption spectra for $(EA)_2CuBr_4$ at visible and IR wavelengths, showing the redshift of the band gap with increasing pressure up to 60 GPa. The d–d (gray arrow) and LMCT transitions (black arrow) are clearly resolved at lower pressures. B) Estimated band gaps from the absorbance spectra in (A) as a function of pressure. Dotted lines indicate structural transition pressures, which coincide with changes in the slope. C) Variable-pressure conductivity of $(EA)_2CuBr_4$ (purple), compared to (EDBE)$CuCl_4$ (green; Ref. [1f]). The gray area denotes the lack of measurable conductivity (σ) below 2.6 GPa ($\sigma < 10^{-8}$ S cm^{-1}).

We then obtained variable-pressure four-point conductivity (σ) measurements (Figure 3C). Notably, the inflection points in the compression-induced conductivity also agree well with structural and optical changes we observe through PXRD and absorption spectroscopy, respectively. We were unable to measure conductivity up to 2.6 GPa due to high sample resistance ($\sigma < 10^{-8}$ S cm^{-1}). At 2.6 GPa, coinciding with the completion of the $\alpha \rightarrow \beta$ phase transition, we observe a sudden conductivity onset with a notably high value of $1.98(8) \times 10^{-3}$ S cm^{-1}. For comparison, this conductivity value is an order of magnitude higher than the maximum measured value for the Cu–Cl perovskite (EDBE)$CuCl_4$ at 51 GPa.[1f] With continued compression, the conductivity of $(EA)_2CuBr_4$ is invariant until it begins to slowly decrease above 6.3 GPa, tracking with the $\gamma \rightarrow \delta$ phase transition. This is followed by rapid reduction of conductivity above 10 GPa, reaching a local minimum at 17 GPa. The sudden drop in conductivity between 10–20 GPa roughly coincides with the plateau in the band gap vs. *P*. Indeed, the rise of the amorphous baseline in the XRD data for the δ phase suggests lattice disorder, which can disrupt electronic conductivity.

We then see a rapid rise in conductivity, increasing by three orders of magnitude with compression from 17 GPa up to ca. 30 GPa. At these high pressures, we expect the effects of Cu–Br bond compression to dominate, leading to increased band dispersion and decreased band gap, reflected in the steadily decreasing band gap at pressures above 20 GPa. The rate of conductivity increase with rising pressure slows above 30 GPa, approaching asymptotic behavior. We measure a maximum conductivity of 0.17(1) S cm^{-1} at 59 GPa. For comparison, despite the higher dimensionality in the 3D perovskite $(CH_3NH_3)PbI_3$, it shows a comparable conductivity of 0.57 S cm^{-1} at 50 GPa (prior to metallization at ca. 62 GPa).[7b] An Arrhenius fit to variable-temperature conductivity values yields an activation energy of conduction (E_a) of 0.106(2) eV for $(EA)_2CuBr_4$ at 59 GPa (Figure S9), consistent with semiconductor-like conduction behavior. The trends exhibited during compression are maintained during decompression as well (Figure S10), consistent with the reversible optical and structural trends observed in other halide perovskites.[1f,7a,b]

Electronic Structure of $(EA)_2CuBr_4$

We performed first-principles-based density functional theory (DFT) calculations, using the projector augmented wave formalism (PAW) as implemented in the VASP code[9] to further interrogate the electronic properties of $(EA)_2CuBr_4$ beyond the simplified schematic in Figure 1C. Structural relaxations were performed with the generalized gradient approximation of Perdew, Burke, and Ernzerhof (PBE)[10] using Tkatchenko–Scheffler[11] van der Waals' corrections (PBE + TS vdW). Comparing calculated total energies for nonmagnetic, ferromagnetic (FM), and antiferromagnetic (AFM) orderings, FM order was found to be energetically preferred, as observed experimentally below a T_c of 11 K[5] (see Supporting Information and Figure S12). For both FM and AFM orderings, a similar electronic structure is observed that is consistent with the schematic depiction in Figure 1C (see Supporting Information). Antiferromagnetic ordering could be considered to more closely approximate the paramagnetism of the perovskite above its T_c. Thus, given the overall similarity in electronic properties between the FM and AFM states in terms of orbital contributions and energy ordering of their densities of states, and the small energetic difference between these two states (see Supporting Information and Figure S16), we show the computed density of states (DOS) of the AFM ordered state at zero pressure in Figure 1D. Here, a Hubbard *U* correction[12] of 8 eV on the Cu d orbitals was included to account for the on-site Coulomb repulsion of localized electrons. The computed DOS is qualitatively consistent with Laporte forbidden Cu d–d transitions as the lowest-energy transition, although the states involved also have significant halide character, as expected for antibonding metal-ligand orbitals. The next-highest-energy occupied states below the Fermi energy have majority Br p character, which are consistent with dipole-allowed transitions to the conduction band minimum (CBM) and a notional LMCT gap. The next set of empty states are 4 eV above the CBM.

We quantify orbital contributions using hybrid Heyd–Scuseria–Ernzerhof (HSE)[13] functional calculations of the DOS for the energetically preferred FM phase at zero pressure (see Supporting Information and Figure S13), which agree well with our PBE + vdW + U calculations (Figure 1D). We find that the Cu d states are spin split, with spin-up and spin-down orbitals below and above the Fermi energy, respectively. The highest-energy filled state has 75% Br p orbital character and 22% Cu d character whereas the CBM has, within our DFT-HSE calculations, 63% Cu d orbital character and 35% Br p contributions. In the analogous Cu–Cl perovskite (Figure S14), the relative contributions of Cl and Cu states in the CBM are 30% and 69% respectively, and the highest filled state has 27% Cu d character and 72% Cl p character, consistent with prior calculations.[14,15] The slightly greater halide contribution in the predominantly d-orbital bands of the Cu–Br perovskites compared to the Cu–Cl perovskites corroborates the hypothesis that the Br compound possesses greater covalency.

We performed constant-pressure relaxations at several fixed pressure values including ambient pressure. The cell volume and internal coordinates were optimized using PBE + TS vdW—again with $U = 8$ eV on the Cu d orbitals. Here for consistency with the DFT FM ground state, we considered only FM ordering. Within the predicted pressure stability range of the α phase below 2.6 GPa, we note a slight reduction in both the JT distortion and octahedral tilting with increased pressure. We find the ratio of long and short equatorial bond lengths from our DFT calculations for the Cu–Br octahedra to be reduced from 1.28 to 1.17. The slightly decreased octahedral tilting is evidenced by the increase of the in-plane Cu-Br-Cu angle from 160° to 165°. At a computed pressure of 20 GPa, the DFT-relaxed α-phase structure continues to exhibit a reduction in JT distortion, approaching nearly equal equatorial bond lengths, with a bond length ratio of 1.03. The computed in-plane Cu-Br-Cu angle increases slightly to 168°. The experimentally observed phase transitions that are likely

associated with large changes in octahedral tilting are not captured in these calculations and could not be considered here without knowledge of the atomic coordinates of the β and γ phases. However, we find that ferromagnetic ordering is no longer preferred above 10 GPa (Figure S18), indicating a magnetic-nonmagnetic transition. Thus, loss of ferromagnetism is consistent with the loss of orthogonality between the primarily $d_{x^2-y^2}$ orbitals, suggesting this as a possible explanation of the emergence of greater conductivity as the JT distortion is further suppressed.

Conclusion

Layered Cu–Cl perovskites have shown appreciable electronic conductivity of 10^{-4} S cm^{-1} only at pressures exceeding 50 GPa, whereas their conductivity is ca. 10^{-9} at 7 GPa. Herein we demonstrate a six-order-of-magnitude increase in conductivity in copper-halide perovskites upon moderate compression, through replacement of Cl with Br. A conductivity of 10^{-3} S cm^{-1} can be obtained in layered Cu–Br perovskites at only 2.6 GPa, with the highest conductivity of 10^{-1} S cm^{-1} measured at 59 GPa. These dramatic improvements in pressured-induced properties may be attributed to increased orbital overlap due to higher-energy and more diffuse Br orbitals relative to the Cl analogs. The lower K_0 of $(EA)_2CuCl_4$ (8.4 GPa)[1c] compared to that of $(EDBE)CuCl_4$ (17.1(4) GPa)[1f] further suggest that the organic bilayers in $(EA)_2CuBr_4$ also contribute to the perovskite's facile structural response to mechanical compression.

We attribute the sudden onset of electronic conductivity at 2.6 GPa in $(EA)_2CuBr_4$ to octahedral tilting in the α → β phase transition that can partially remove the orthogonality between singly occupied $d_{x^2-y^2}$-derived orbitals and provide a conduction pathway, albeit with thinly dispersed electronic bands. If the conductivity were to arise instead from thermal promotion of electrons across a 1.6 eV band gap, a conservative estimate yields a carrier concentration below 10^6 cm^{-3} (Figure S19). To then achieve a conductivity of 10^{-3} S cm^{-1}, carrier mobilities would have to be non-physically high (10^{10} cm^2 V^{-1} s^{-1}; see Supporting Information). Even at 20 GPa, where the conductivity begins to rise again and the band gap is ca. 1.0 eV, conservative estimates give a carrier concentration of 10^{10} cm^{-3} and necessitate highly unlikely mobilities of 5×10^4 cm^2 V^{-1} s^{-1}. Thus, the sudden onset of conductivity is more likely due to the pressure-induced formation of half-filled electronic bands by partially relieving the orthogonality between singly occupied molecular orbitals composed of Cu d and Br p orbitals. At higher pressures, particularly in the γ phase when the perovskite's compressibility suddenly decreases ca. 2.5-fold, we expect Cu–Br bond compression to drive the increase in conductivity through both a reduction in band gap and increase in band dispersion.

We previously discussed the possibility of using the reversible pressure-induced changes in perovskite films for printing transient electronic circuits through high-pressure contact and registering impact or strain through perovskite coatings.[16] The enhanced pressure response of Cu–Br perovskites bring the pressures required for such switching behavior to technologically accessible values.

Acknowledgements

The experimental work was supported by the Department of Energy (DOE), Office of Basic Energy Sciences (BES), Division of Materials Sciences and Engineering, under contract DE-AC02-76SF00515. DFT calculations were supported by the DOE, Office of Science, Office of BES (Theory of Materials FWP) Materials Sciences and Engineering Division (DE-AC02-05CH11231). Computational resources used at the Molecular Foundry were supported by the DOE, Office of Science, Office of BES under contract no. DE-AC02-05CH11231. Additional computational resources were provided by NERSC. A.J. is grateful for the Stanford Interdisciplinary Graduate Fellowship and the William S. Johnson Fellowship from the Department of Chemistry. High-pressure absorption spectra were collected at the Infrared Laboratory of the National Synchrotron Light Source II (NSLS II), a DOE Office of Science User Facility operated by Brookhaven National Laboratory (BNL) (DE-SC0012704). The Infrared Laboratory is supported by the Consortium for Materials Properties Research in Earth Sciences (COMPRES) under the National Science Foundation (NSF) Cooperative Agreement EAR 1606856 and the DOE/National Nuclear Security Administration (DE-NA-0002006), Carnegie DOE Alliance Center. High-pressure PXRD data were collected at beamline 12.2.2 at the Advanced Light Source (ALS). The ALS is supported by the Director, Office of Science, Office of BES of the DOE (DE-AC02-05CH11231). The high-pressure facilities at the ALS are supported by COMPRES under NSF Cooperative Agreement EAR 11–57758. We thank Dr. Zhenxian Liu at the Infrared Laboratory, Drs. Martin Kunz and Christine Beavers at the ALS, and Sam Girdzis for experimental assistance and Drs. Jung-Hoon Lee, Sinéad Griffin, and Marina Filip for useful discussions.

Conflict of interest

The authors declare no conflict of interest.

Keywords: conducting materials · high-pressure chemistry · Jahn–Teller distortion · layered copper halide perovskite · semiconductors

How to cite: *Angew. Chem. Int. Ed.* **2020**, *59*, 4017–4022
Angew. Chem. **2020**, *132*, 4046–4051

[1] a) Y. Moritomo, Y. Tokura, *J. Chem. Phys.* **1994**, *101*, 1763–1766; b) R. Valiente, F. Rodríguez, *Phys. Rev. B Condens. Matter Mater. Phys.* **1999**, *60*, 9423–9429; c) K. Ohwada, K. Ishii, T. Inami, Y. Murakami, T. Shobu, H. Ohsumi, N. Ikeda, Y. Ohishi, *Phys. Rev. B Condens. Matter Mater. Phys.* **2005**, *72*, 014123; d) F. Rodríguez, F. Aguado, R. Valiente, M. Hanfland, J. P. Itiè, *Phys.*

Status Solidi B **2007**, *244*, 156 – 161; e) F. Aguado, F. Rodríguez, R. Valiente, J.-P. Itiè, M. Hanfland, *Phys. Rev. B Condens. Matter Mater. Phys.* **2012**, *85*, 100101; f) A. Jaffe, Y. Lin, W. L. Mao, H. I. Karunadasa, *J. Am. Chem. Soc.* **2015**, *137*, 1673 – 1678; g) P. Ghalsasi, N. Garg, M. N. Deo, A. Garg, H. Mande, P. Ghalsasi, S. M. Sharma, *Phys. Chem. Chem. Phys.* **2015**, *17*, 32204 – 32210; h) Q. Li, S. Li, K. Wang, Z. Quan, Y. Meng, B. Zou, *J. Phys. Chem. Lett.* **2017**, *8*, 500 – 506.

[2] a) L. Gao, Y. Y. Xue, F. Chen, Q. Xiong, R. L. Meng, D. Ramirez, C. W. Chu, J. H. Eggert, H. K. Mao, *Phys. Rev. B Condens. Matter Mater. Phys.* **1994**, *50*, 4260 – 4263; b) C. Murayama, Y. Iye, T. Enomoto, N. Môri, Y. Yamada, T. Matsumoto, Y. Kubo, Y. Shimakawa, T. Manako, *Physica C* **1991**, *183*, 277 – 285; c) J. S. Schilling, in *Frontiers of High Pressure Research II: Application of High Pressure to Low-Dimensional Novel Electronic Materials*, *Vol. 48* (Eds.: H. D. Hochheimer, B. Kuchta, P. K. Dorhout, J. L. Yarger), Springer, New York, **2001**, pp. 345 – 360.

[3] a) R. Willett, H. Place, M. Middleton, *J. Am. Chem. Soc.* **1988**, *110*, 8639 – 8650; b) R. Willett, *Acta Crystallogr. Sect. B* **1990**, *46*, 565 – 568.

[4] D. B. Mitzi in *Progress in Inorganic Chemistry*, *Vol. 48*, Wiley-VCH, Weinheim, **1999**, pp. 1 – 121.

[5] L. J. de Jongh, A. R. Miedema, *Adv. Phys.* **1974**, *23*, 1 – 260.

[6] G. S. Long, M. Wei, R. D. Willett, *Inorg. Chem.* **1997**, *36*, 3102 – 3107.

[7] a) A. Jaffe, Y. Lin, C. M. Beavers, J. Voss, W. L. Mao, H. I. Karunadasa, *ACS Cent. Sci.* **2016**, *2*, 201 – 209; b) A. Jaffe, Y. Lin, W. L. Mao, H. I. Karunadasa, *J. Am. Chem. Soc.* **2017**, *139*, 4330 – 4333; c) Y. Lee, D. B. Mitzi, P. W. Barnes, T. Vogt, *Phys. Rev. B Condens. Matter Mater. Phys.* **2003**, *68*, 020103.

[8] a) S. R. Desjardins, K. W. Penfield, S. L. Cohen, R. L. Musselman, E. I. Solomon, *J. Am. Chem. Soc.* **1983**, *105*, 4590 – 4603; b) S. R. Desjardins, D. E. Wilcox, R. L. Musselman, E. I. Solomon, *Inorg. Chem.* **1987**, *26*, 288 – 300.

[9] G. Kresse, J. Furthmüller, *Phys. Rev. B Condens. Matter Mater. Phys.* **1996**, *54*, 11169 – 11186.

[10] J. P. Perdew, K. Burke, M. Ernzerhof, *Phys. Rev. Lett.* **1996**, *77*, 3865 – 3868.

[11] A. Tkatchenko, M. Scheffler, *Phys. Rev. Lett.* **2009**, *102*, 073005.

[12] S. L. Dudarev, G. A. Botton, S. Y. Savrasov, C. J. Humphreys, A. P. Sutton, *Phys. Rev. B Condens. Matter Mater. Phys.* **1998**, *57*, 1505 – 1509.

[13] A. V. Krukau, O. A. Vydrov, A. F. Izmaylov, G. E. Scuseria, *J. Chem. Phys.* **2006**, *125*, 224106.

[14] S. Gupta, T. Pandey, A. K. Singh, *Inorg. Chem.* **2016**, *55*, 6817 – 6824.

[15] a) P. Zolfaghari, G. A. de Wijs, R. A. de Groot, *J. Phys. Condens. Matter* **2013**, *25*, 295502; b) D. Cortecchia, H. A. Dewi, J. Yin, A. Bruno, S. Chen, T. Baikie, P. P. Boix, M. Grätzel, S. Mhaisalkar, C. Soci, N. Mathews, *Inorg. Chem.* **2016**, *55*, 1044 – 1052.

[16] A. Jaffe, Y. Lin, H. I. Karunadasa, *ACS Energy Lett.* **2017**, *2*, 1549 – 1555.

Manuscript received: October 1, 2019
Accepted manuscript online: December 27, 2019
Version of record online: January 24, 2020

